



Research papers

Delineate the unknown aquifer geometry and boundary condition using hydraulic tomography

Mpendulo Mangaliso Mtsetfwa^{a,b}, Zaiyong Zhang^{c,d}, Chengcheng Gong^e, Hong-Ru Lin^f ,
Jet-Chau Wen^{f,g}, Yu-Li Wang^{a,*} 

^a Department of Bioenvironmental Systems Engineering, National Taiwan University, Taiwan

^b Now at Joint River Basin Authorities – Project Board, Eswatini

^c Key Laboratory of Subsurface Hydrology and Ecological Effects in Arid Region, Chang'an University, China

^d School of Water and Environment, Chang'an University, China

^e Key Laboratory of Ecological Safety and Sustainable Development in Arid Lands, Northwest Institute of Eco-Environment and Resources, Chinese Academy of Sciences, China

^f Research Center for Soil and Water Resources and Natural Disaster Prevention, National Yunlin University of Science and Technology, Taiwan

^g Department of Safety, Health and Environmental Engineering, National Yunlin University of Science and Technology, Taiwan

ARTICLE INFO

This manuscript was handled by Corrado Corradini, Editor-in-Chief, with the assistance of Gabriele Chiogna, Associate Editor

Keywords:

Inversion

Hydraulic Tomography

Groundwater

ABSTRACT

The geometric shape and boundary conditions of an aquifer are vital properties in many aspects of studies in water resources and hydrogeology. An accurate characterization of these hydraulic properties can help stakeholders manage water resources effectively and mitigate the negative impact of overexploited water resources on the environment. However, due to the complex subsurface hydrogeological characteristics and limited observations, it is challenging to effectively characterize the aquifer's geometric shape and boundary conditions. This study investigates the effectiveness of hydraulic tomography to identify unknown aquifer geometry and boundary conditions using a sandbox experiment. The results show that when the true no flux boundary is incorrectly assigned as a constant head, the low hydraulic conductivity (K) and high specific storage (S_s) zones manifest along the boundaries. The low K anomaly acts as an impermeable barrier, while the high S_s anomaly behaves as a water tank to prevent water flowing into the sandbox. Conversely, it is challenging to use the anomalous K and S_s zones to identify the constant head boundary when it is incorrectly assigned as a no flux. The estimated K values remain similar to those with the correct boundary while both anomalously high and low S_s values manifest in the vicinity of incorrectly assigned boundary. Therefore, to prevent misinterpretation, a constant head boundary should be used when the boundary condition is unknown. In addition, the transient state measurements provide a more reliable assessment of boundary conditions than the steady state measurements. The partially redundant temporal measurements offset the influences of measurement noise. Finally, the hydraulic tomography is effective in identifying no flux boundary conditions when both aquifer geometry and boundary type are unknown. The low K and S_s anomalies emerge near the locations of true no flux boundaries. However, identifying constant head boundary remains a challenge, as the K and S_s anomalies did not clearly correspond to the actual locations of constant head boundaries. These analyses aid in developing strategies to specify the unknown aquifer geometry and boundary conditions, enabling scenario analysis of regional water resources management.

1. Introduction

The aquifer geometric shape and boundary conditions are vital properties in hydrogeological and water resources studies. These aquifer characteristics dominate groundwater recharge rates and their

sensitivity to climate change (Hartmann et al., 2017), influence the direction and flux of solute transport (Michael and Khan, 2016), and help managers understand aquifer behaviors and manage water resources (Adeyeri et al., 2024). Because of the limited underground monitoring tools, sparse measurements, and model structure error (Ho et al., 2021;

* Corresponding author.

E-mail address: ylwang@ntu.edu.tw (Y.-L. Wang).

<https://doi.org/10.1016/j.jhydrol.2025.132754>

Received 28 October 2024; Received in revised form 28 December 2024; Accepted 15 January 2025

Available online 26 January 2025

0022-1694/© 2025 Elsevier B.V. All rights are reserved, including those for text and data mining, AI training, and similar technologies.

Ren et al., 2021), the aquifer geometry and boundary conditions are usually unclear. Without this hydraulic information, the flow and solute transport predictions often deviate from the reality in the forward and inverse modelings (Zhang et al., 2014). The misinterpreted flow and transport pathways deteriorate the effectiveness of water resources management (Zhang et al., 2018) and contaminant remediation (Zhang et al., 2024). As such, an accurate characterization of these hydraulic properties is critical.

Over the past few decades, efforts have been devoted to developing the modeling frameworks with uncertain boundary conditions (Irsa and Zhang, 2012; Sun et al., 2013; Zhang, 2014; Jiao and Zhang, 2014a, 2014b, 2015; Coelho et al., 2017; Bastani and Harter, 2020). Among these methods, hydraulic tomography (HT) is one of the advanced approaches to effectively extract information of aquifer geometry and boundary conditions embedded in the limited observations (Sun et al., 2013; Daranond et al., 2020; Liu et al., 2020; Su et al., 2024). The HT method is based on the principles of tomographic survey, in which a series of hydraulic tests are conducted at different locations of an aquifer to characterize the spatial variability of aquifer hydraulic properties (Lin et al., 2023).

All the previous studies utilized synthetic experiments to investigate the potential of HT to characterize the aquifer geometry and type of boundary. Sun et al. (2013) investigated the impact of incorrectly specified boundary conditions on the spatial distribution of aquifer hydraulic parameters. They suggested that a low permeable zone manifested in front of the incorrectly specified constant head boundary can be used to approximate the distant impermeable boundary. Daranond et al. (2020) explored the effect of unknown aquifer geometry on estimating the spatial distributions of hydraulic conductivity (K) and specific storage (S_s) using synthetic sequential pumping tests. They found that unknown impermeable boundaries reduce the estimated K values in the vicinity of the unknown boundary, whereas the estimated S_s values and their spatial distribution remain affected. Liu et al. (2020) expanded Daranond et al. (2020)'s method to a synthetic watershed-scale aquifer. In contrast to the findings of Daranond et al. (2020), Liu et al. (2020) found that the anomalous high K and S_s areas can be utilized to identify the location of constant head boundaries. Conversely, the low K and S_s areas indicate the presence of impermeable boundaries. These inconsistent findings suggest that identifying the type and location of an unknown aquifer boundary using HT remains inconclusive. Analysis of the laboratory and field datasets is necessary to examine the findings from the synthetic experiments.

Furthermore, it remains unclear whether the steady state or transient state HT is more effective in identifying the boundary condition. For example, Liu et al. (2020) suggested that the steady state HT is more effective than the transient state HT, as the former requires fewer constraints than the latter to formulate a well-defined problem. However, the results presented by Liu et al. (2020) are based on analyses conducted using noise-free synthetic experiments. In practice, measurements inevitably contain noise. While temporal observations are capable of cancelling out the effects of random noise, this is not the case with steady state observations. Therefore, it is necessary to examine whether the same conclusion holds in the real-world situation.

To address the above issues, this paper designs a sandbox experiment to investigate and examine the potential of HT to identify the unknown aquifer boundary condition and geometry. Specifically, this study aims to: (1) examine to what extent do the anomalous K and S_s can be used to identify the aquifer geometry and type of unknown boundary, (2) evaluate the effectiveness of steady and transient state HT on characterizing the aquifer geometry and boundary condition using groundwater level measurements, and (3) investigate the effects of well location and density on identifying the boundary. To accomplish these objectives, we built a sandbox experiment and tested the ability of anomalous K and S_s zones to capture the boundary type and aquifer geometry by comparing the estimated K and S_s tomograms using the incorrectly assigned boundary conditions to those using the correct

boundary conditions. We then explore the effects of well location and density on identifying the boundary conditions. These analyses aid in developing strategies to specify the unknown aquifer geometry and boundary conditions for scenario analysis of regional water resources management.

2. Methods

2.1. Sandbox experiment

A sandbox was set up in the laboratory. The sandbox is 170 cm in length, 97.5 cm in height, and 10 cm in width (Fig. 1a). The sandbox is filled with quartz consisting of various grain sizes ranging from 0.2 cm to 0.007 cm (particles remaining on sieve #20 to #200, Fig. 1b). There are 45 holes (5 rows and 9 columns) installed. These holes are located 12.5, 30.5, 48.5, 66.5, and 84.5 cm below the top boundary. They serve as screens for partially penetrating wells. The 45 pressure transducers (monitoring range: 0–3 m, instrument error: $\pm 0.2\%$ Full Scale) were connected to the holes with tubes respectively to measure the water pressure variations. A pump was used to extract the water from the sandbox. This pump can be connected to any well that serves as a pumping well.

The top and bottom boundaries of the sandbox are no flux boundaries. There are three plates (i.e., top, middle, and bottom) installed on the left and right sides, respectively. The top and bottom plates are constant head boundaries while the middle plates are set as no flux (Fig. 1c). A reservoir is placed next to the plate and followed by an overflow tank. The reservoir and tank are connected by tubes. By manipulating the water table of the overflow tank, the water level of the reservoirs on both sides of the sandbox (constant head boundaries) can be adjusted. The purpose of using a reservoir and an overflow tank to store the water is to minimize the water level fluctuations at the constant head boundary. The water tables of the left and right reservoirs were set to be 140 cm in height. The sandbox was fully saturated. The aquifer was under a hydrostatic condition before pumping was implemented.

The 45 constant-rate pumping tests are conducted sequentially. The pumping rates were set between 4.76 mL/s and 20.18 mL/s to avoid the negative pressure (unsaturated zone around the pumping well and the top of the sandbox) and the small signal-to-noise ratio (large enough drawdown in distant regions). During each pumping test, the groundwater level variations were recorded every 2 s from the 45 observation wells. Pumping stopped when the flow field reached a steady state. A total of 45×45 drawdown curves were recorded.

2.2. Groundwater flow models

A 2-D steady state groundwater flow in a vertical heterogeneous aquifer is employed. It can be expressed as

$$\nabla \cdot [K(\mathbf{x}) \nabla H(\mathbf{x}, t)] = Q(\mathbf{x}, t) \quad (1)$$

and a transient state flow is expressed as

$$\nabla \cdot [K(\mathbf{x}) \nabla H(\mathbf{x}, t)] = S_s(\mathbf{x}) \frac{\partial H(\mathbf{x}, t)}{\partial t} + Q(\mathbf{x}, t) \quad (2)$$

subject to the initial and boundary conditions

$$H|_{\Gamma_1} = H(\mathbf{x}, t), \quad q|_{\Gamma_2} = q(\mathbf{x}, t), \quad \text{and} \quad H = H(\mathbf{x}, t_0) \quad (3)$$

where H is the total head (L), K is the hydraulic conductivity (L/T), S_s is the specific storage (1/L), \mathbf{x} is the vector in x and z directions, t is the time, t_0 is the initial time, Q is the source and sink term (1/T), Γ_1 is the prescribed head at the Dirichlet boundary, and Γ_2 is the prescribed flux at the Neumann boundary.

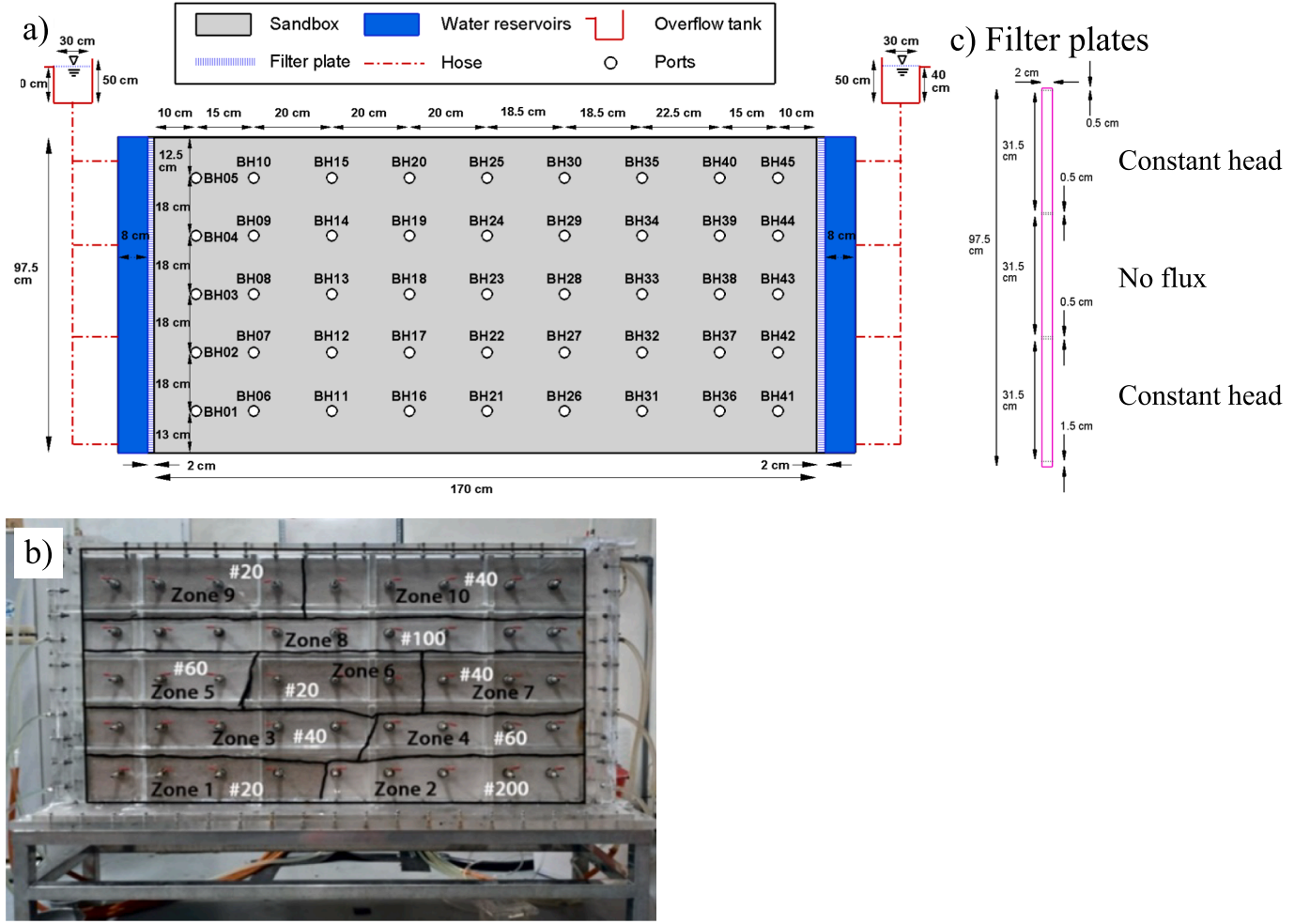


Fig. 1. a) The sandbox configuration. b) The sandbox is filled with quartz consisting of various grain sizes (a heterogeneous aquifer). c) Three filter plates (top, middle, and bottom) on the right and left boundaries.

2.3. Inverse algorithm for tomographic survey

We employ the successive linear estimator (SLE), a widely used inverse algorithm for HT (Wang et al., 2019; Wang et al., 2022), to characterize the boundary condition and geometric shape of an aquifer. The SLE is built upon the stochastic conditional expectation (Priestley, 1982) and the hydrogeology cokriging (Kitanidis and Vomvoris, 1983; Dagan, 1985). This method employs the iterative approach to extract the underlying subsurface hydraulic characteristics embedded in the hydrological measurements (Kitanidis, 1995; Yeh et al., 1995).

The SLE considers hydraulic parameters (e.g., K and Ss) as a spatial stochastic process characterized by statistical information such as mean, variance, and spatial correlation function. The estimated parameter field is iteratively determined by incorporating the differences between observed and simulated head, and the sensitivity of the head with respect to parameter. The iterative linear estimator is:

$$\hat{\mathbf{f}}^{(r+1)} = \hat{\mathbf{f}}^{(r)} + \omega^{(r)}[\mathbf{h}^* - \mathbf{h}^{(r)}] \quad (4)$$

in which $\hat{\mathbf{f}}^{(r)}$ ($n_f \times 1$) is the estimated K (or Ss), \mathbf{h}^* ($n_d \times 1$) is the observed head, $\mathbf{h}^{(r)}$ ($n_d \times 1$) is the simulated head based on the estimated parameters from the r^{th} iteration, n_f is the number of elements, n_d is the number of observations, and the superscript r is the iteration index starting from zero. $\omega^{(r)}$ ($n_f \times n_d$) is a weighting matrix that links heads and parameters. This weighting matrix is solved by:

$$\omega^{(r)}[\boldsymbol{\varepsilon}_{hh}^{(r)} + \boldsymbol{\theta}^{(r)}\mathbf{I}] = \boldsymbol{\varepsilon}_{fh}^{(r)} \quad (5)$$

where $\boldsymbol{\varepsilon}_{hh}^{(r)}$ ($n_f \times n_d$) is the covariance matrix of head at r^{th} iteration and $\boldsymbol{\varepsilon}_{fh}^{(r)}$ is the covariance matrix of head to K (or Ss). \mathbf{I} is the identity matrix. The term $\boldsymbol{\theta}^{(r)}$ is a dynamic stabilizer that ensures numerical stability of solving an inverse matrix. We utilize the Levenberg-Marquardt algorithm to leverage the computation cost.

The covariance matrices $\boldsymbol{\varepsilon}_{hh}^{(r)}$ and $\boldsymbol{\varepsilon}_{fh}^{(r)}$ are derived from the first-order approximation (Gao et al., 2018):

$$\boldsymbol{\varepsilon}_{hh}^{(r)} = \mathbf{J}_{fh}^{(r)T} \boldsymbol{\varepsilon}_{ff}^{(r)} \mathbf{J}_{fh}^{(r)} \text{ and } \boldsymbol{\varepsilon}_{fh}^{(r)} = \boldsymbol{\varepsilon}_{ff}^{(r)} \mathbf{J}_{fh}^{(r)} \quad (6)$$

in which $\mathbf{J}_{fh}^{(r)}$ ($n_f \times n_d$) is the sensitivity of the head to the estimated parameters during the r^{th} iteration. The sensitivity is evaluated by the adjoint approach (Sykes et al., 1985; Sun and Yeh, 1990). This method is effective when the number of estimated parameters is much larger than the number of observations. $\boldsymbol{\varepsilon}_{ff}^{(r)}$ ($n_f \times n_f$) is the residual covariance matrix of K (or Ss) at r^{th} iteration and is given by:

$$\boldsymbol{\varepsilon}_{ff}^{(r+1)} = \boldsymbol{\varepsilon}_{ff}^{(r)} - \omega^{(r)} \boldsymbol{\varepsilon}_{fh}^{(r)T} \quad (7)$$

The diagonal terms of $\boldsymbol{\varepsilon}_{ff}^{(r)}$ represent the uncertainty of the parameters, while the off-diagonal terms represent the cross-covariances between parameters. They quantify the uncertainty and correlation between the

estimated parameters. At iteration $r = 0$, $\epsilon_{ff}^{(r)}$ is constructed based on the prior geological knowledge of K (or S_s) using variances, correlation lengths, and covariance functions (e.g., kriging).

The iteration terminates when either the maximum number of iterations is reached or the difference between the simulated and observed head is smaller than a user-specified value. Appropriate tolerance prevents overfitting and ensures convergence of the solution.

SLE starts with some geostatistical information on K (or S_s) parameters, such as the mean, variance, and correlation scale. It then fuses the water level information by iteratively updating the conditional mean K and S_s fields and their covariance function. The estimated field, conditioned on the given datasets, is an unbiased mean estimate and has the smallest uncertainty (Gao et al., 2021; Wang et al., 2021).

2.4. Scenarios analyzed

2.4.1. Model setups

The sandbox is discretized by 2.5 (cm) × 2.5 (cm) grids. For scenarios 1 to 12 (see section 2.4.2), there are 68 × 39 grids. The initial water level is 140 (cm). The constant head boundary is set to 140 (cm). For scenario 13 (i.e., an extended domain that is broader than the size of the sandbox), there are 100 × 59 grids. The initial water level and the constant head boundary are set to 160 (cm). For the inversion of each scenario, the initial mean K is 0.04 (cm/s), and the mean S_s is 0.0007 (1/cm). The exponential variogram is used to construct the prior covariance matrix. The correlation length of $\ln K$ and $\ln S_s$ along the x and z directions are 85 (cm) and 20 (cm), and the variances of $\ln K$ and $\ln S_s$ are 1 (–).

2.4.2. Aquifer geometry and boundary conditions

Thirteen scenarios are designed to identify the boundary conditions (scenarios 1 to 12) and geometric shape (scenario 13) of an aquifer. The scenarios designed are summarized in Table 1.

Scenarios 1 to 6: Steady vs. Transient state HT

Scenarios 1 to 6 evaluate the effectiveness of steady and transient state HT in identifying misassigned constant head and no flux boundaries. The drawdown data collected from 45 observation wells during 45 pumping tests are used.

Scenario 1: The first scenario utilizes the correct boundary (Fig. 2a) and the steady state HT. This scenario assumes that the type and location of boundary are known. This scenario serves as a reference for scenarios 2 and 3.

Scenario 2: The second scenario assumes that the locations of boundaries are known but the types of boundaries are unknown (Fig. 2b). The steady state HT is employed. No flux boundaries are incorrectly assigned as constant head boundaries. This scenario evaluates how the anomalous K values indicate the incorrectly assigned constant head boundary.

Scenario 3: The third scenario also assumes that the locations of boundaries are known but the types of boundaries are unknown (Fig. 2c). The steady state HT is employed. Both constant head and no flux boundaries are misassigned. This scenario evaluates how the anomalous K values relate to the incorrectly assigned no flux boundary.

Table 1

Scenarios designed to understand the effectiveness of identifying the aquifer geometry and boundary conditions. N/A represents not applicable.

Scenario	1	2	3	4	5	6	7	8	9	10	11	12	13
Steady State	✓	✓	✓										
Transient State				✓	✓	✓	✓	✓	✓	✓	✓	✓	✓
Number of wells	45	45	45	45	45	45	15	15	15	10	10	10	45
Correct boundary	✓			✓			✓			✓			N/A
Incorrectly assigned no flux		✓	✓		✓	✓		✓	✓		✓	✓	N/A
Incorrectly assigned constant head			✓			✓			✓			✓	N/A
Unknown aquifer geometry													✓

Scenarios 4 to 6: Configurations identical to those in scenarios 1 to 3 but with transient state HT. Scenario 4 serves as a reference for scenarios 5 and 6. These scenarios evaluate how the anomalous K and S_s values indicate the incorrectly assigned constant head or no flux boundaries.

Scenarios 7 to 12: Influence of well networks

Scenarios 7 to 12 examine the impact of well positioning and density on identifying misassigned boundary conditions. These scenarios use drawdown data from three different well networks (45, 15, and 10 wells). The first well network (scenarios 4 to 6) includes 45 pumping and observation wells and serves as a reference (Fig. 3a). The second well network (scenarios 7 to 9) uses 15 pumping and observation wells, encompassing the boundaries and the central linear well array (Fig. 3b). The third well network (scenarios 10 to 12) utilizes 10 pumping and observation wells, with wells located along the left- and right-hand side boundaries (Fig. 3c). This well network is used to ascertain whether focusing on the localized boundary region helps identify the type of boundary as accurately as those using denser networks.

Scenarios 7 to 9: Configurations identical to those in scenarios 4 to 6 but with 15 wells.

Scenarios 10 to 12: Configurations identical to those in scenarios 4 to 6 but with 10 wells.

Scenario 13: Unknown aquifer geometry and boundary conditions

Scenario 13 investigates the effectiveness of identifying the unknown aquifer geometry and boundary conditions. An extended domain broader than the sandbox size is used (Fig. 2d). The transient state HT is employed. All boundaries are assigned as constant head boundary conditions. This scenario evaluates the potential for detecting both unknown boundary types and locations.

2.5. Evaluation criteria

2.5.1. Contour maps

The visual comparison provides a preliminary qualitative analysis of the role of anomalous K and S_s in identifying the aquifer geometry and boundary conditions. Visualizing the spatial distributions of K and S_s identify areas where K and S_s anomalies occur.

2.5.2. Percentage difference

The percentage difference (PD) of the estimated K and S_s values of various scenarios (e.g., scenarios 2, 3, 5, and 6) with respect to the reference (e.g., scenarios 1 and 4) quantitatively evaluates to what extent does the K and S_s anomalies characterize the incorrectly assigned boundary conditions. The percentage difference is calculated by

$$PD = \frac{K_{incorrect} - K_{correct}}{K_{correct}} \cdot 100\% \tag{8}$$

where $K_{incorrect}$ is the hydraulic conductivity or specific storage for the incorrectly assigned boundary. $K_{correct}$ is the hydraulic conductivity or specific storage for the correct boundary. Fig. 4 summarizes how the different boundary types and aquifer geometry are identified in the inversion using SLE algorithm.

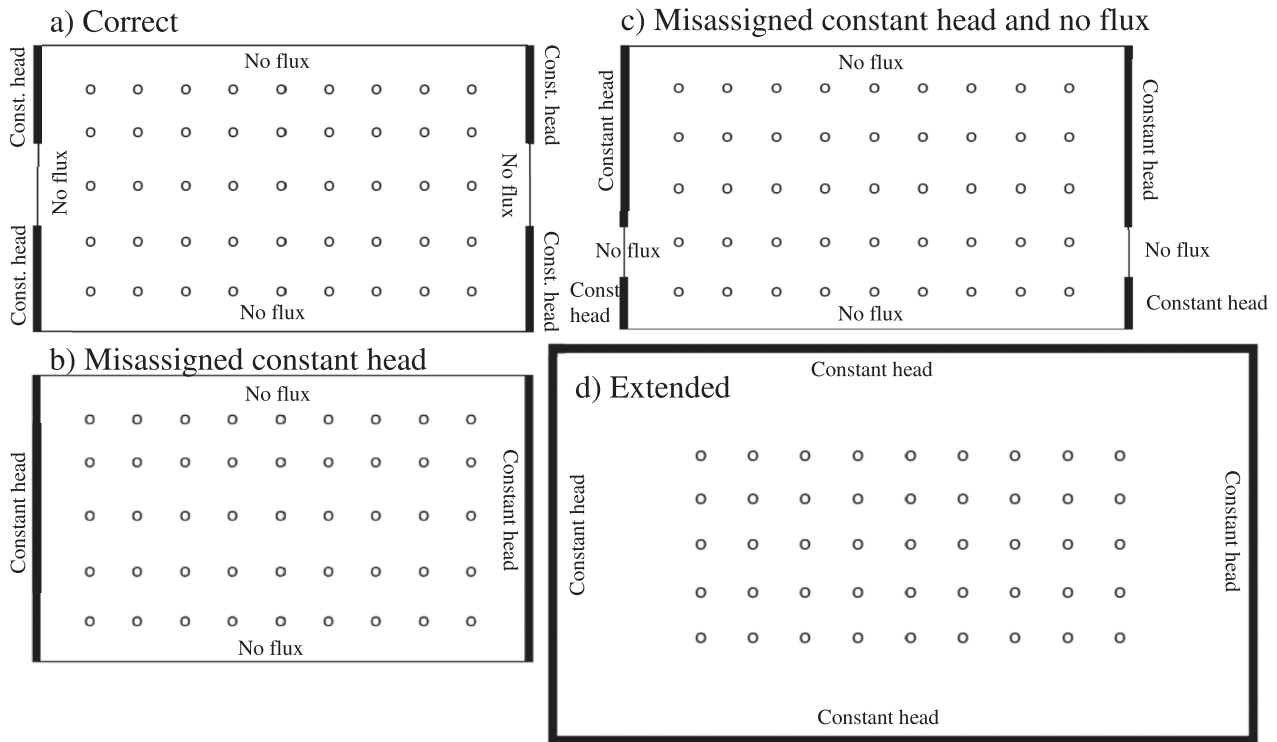


Fig. 2. Different scenarios of boundary conditions. The bold solid lines indicate the constant head boundaries. The remaining boundaries are defined as no flux. a) Correct boundary (scenarios 1, 4, 7, and 10). b) Misassigned constant head boundary (scenarios 2, 5, 8, and 11). c) Misassigned no flux boundary (scenarios 3, 6, 9, and 12). d) The extended domain with constant head on all boundaries (scenario 13). The white circles represent the wells. Note that the number of wells utilized in scenarios 4 to 12 varies. Please refer to Fig. 3 for the details.

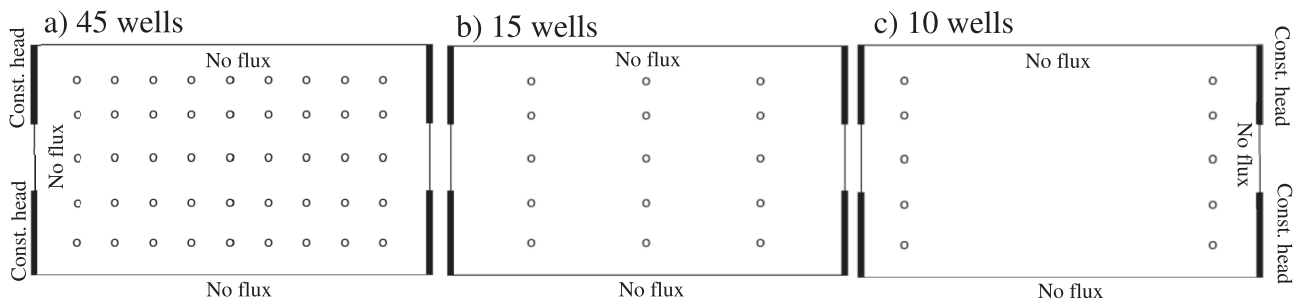


Fig. 3. Different numbers of pumping and observation wells. The white circles represent the wells. a) The well network with 45 pumping and observation wells (scenarios 4 to 6). b) The well network with 15 pumping and observation wells (scenarios 7 to 9). c) The well network with 10 pumping and observation wells (scenarios 10 to 12). The bold solid lines indicate the constant head boundaries. The remaining boundaries are no flux. Note that the boundary conditions utilized in scenarios 4 to 12 vary. Please refer to Fig. 2 for the details.

3. Results and discussions

3.1. Identify the unknown boundary condition using anomalous K and S_s

3.1.1. Effectiveness of steady state HT

Fig. 5a and b present the percentage differences of estimated K values with steady state HT. Fig. 5a illustrates the percentage difference of estimated K values between the incorrectly assigned (scenario 2) and true (scenario 1) types of boundary conditions when the middle plates are incorrectly assigned as the constant head. The K spatial distributions using the true and incorrect boundaries are similar in most zones except for the regions near the boundary. For example, when a constant head boundary is incorrectly assigned, the relatively low K zones emerge near the regions where the true no flux boundary should be (blue areas next to the middle plates in Fig. 5a). These low permeability zones are an important indication of the true boundary type. They act as the no flow

boundary and prevent the water from flowing into the sandbox. The low K anomaly near the incorrectly assigned left-hand side boundary is not as clear as that near the right-hand side boundary. Nevertheless, the estimated K values are still slightly lower than those using the correct type of boundary.

Fig. 5b presents the percentage differences of estimated K values between the incorrectly assigned (scenario 3) and true (scenario 1) types of boundary conditions. The incorrectly assigned boundaries are placed on the middle and the upper half of the bottom plates. When the true constant head boundary is incorrectly assigned as the no flux boundary on the upper half of bottom plates, the estimated K values near the incorrectly assigned boundaries remain similar to those using the correct boundary. This finding aligns with the synthetic experiment of Su et al. (2024). Besides, when the true no flux boundary is incorrectly assigned as the constant head boundary on the middle plates, the anomalous low K zone manifests. Unlike the right-hand side boundary, the anomalies

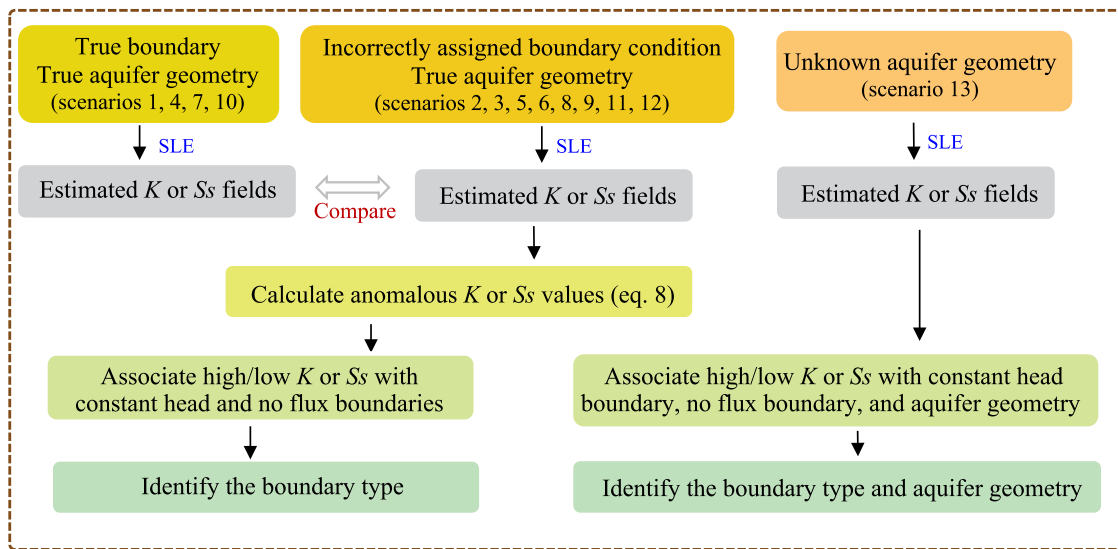


Fig. 4. The flowchart of identifying the boundary conditions and aquifer geometry using anomalous K and S_s estimates.

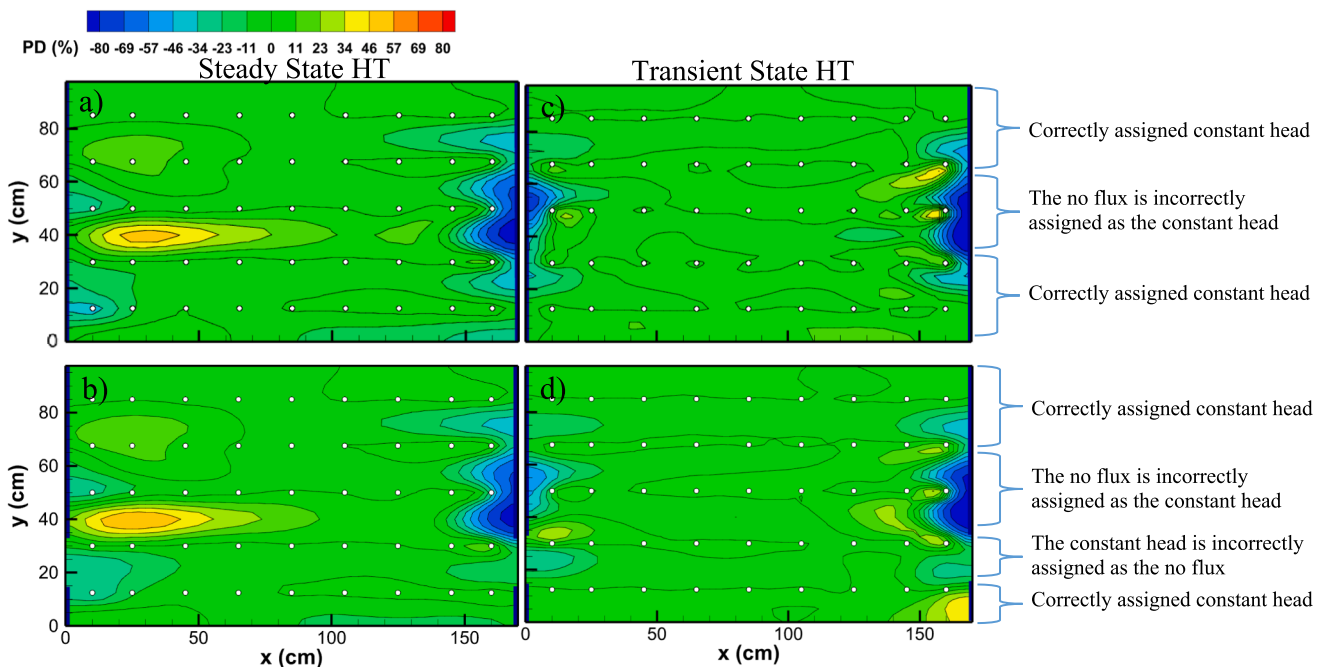


Fig. 5. The percentage differences of estimated K values between the true and incorrectly assigned boundary conditions using the steady state (a and b) and transient state (c and d) pumping tests. The white circles represent the wells. The bold solid lines indicate the constant head boundaries. The remaining boundaries are no flux.

near the left-hand side boundary are not significant. This inconsistency might be due to the noisy measurements. The HT for identifying the boundary condition rests upon the significant change in hydraulic properties near the actual boundaries of a groundwater basin. When using the steady state pumping test, the influences of measurement noise are not able to be cross-validated by other measurements recorded in the same well. Thus, we examine the capability of transient state drawdown to identify the boundary condition in the following session.

3.1.2. Effectiveness of transient state HT

Fig. 5c and d present the percentage differences of estimated K values between the incorrectly assigned (scenarios 5 and 6) and true (scenario 4) boundary conditions with transient state HT. The low K zones manifest on both the left- and right-hand sides of the sandbox to compensate

for the effects of incorrectly assigned constant head boundaries (Fig. 5c). When the true constant head boundary is incorrectly assigned as the no flux boundary on the upper half of bottom plates, the estimated K values near the incorrectly assigned boundaries remain similar to those using the correct boundary (Fig. 5d). A comparison of the percentage differences in estimated K values using transient state drawdowns (Fig. 5c and d) and those using steady state drawdowns (Fig. 5a and b) shows that anomalies are more consistently manifested on both the left- and right-hand sides of the sandbox when transient drawdowns are employed. The effects of incorrectly assigned boundaries on estimated K values in the vicinity of boundary are summarized in Table 2.

Fig. 6 presents the percentage differences of estimated S_s fields using the true (scenario 4) and incorrectly assigned (scenarios 5 and 6) boundaries. When a constant head boundary is incorrectly assigned, a

Table 2

Effects of incorrectly assigned boundary conditions and unknown aquifer geometry. N/A represents not applicable.

	Unknown boundary type		Unknown aquifer geometry and boundary type	
	Constant head	No flux	Constant head	No flux
True boundary	Constant head	No flux	Constant head	No flux
Incorrectly assigned	No flux	Constant head	N/A	N/A
Effects near/on boundary	No impact on K High and Low S_s	Low K High S_s	Not clear	Low K Low S_s

relatively high S_s zone emerges in the vicinity of the region where the true no flux boundary should be present (Fig. 6a and b). The high storage capacity zone is indicative of the true impermeable boundary. It functions as a water tank to prevent the water from flowing into the sandbox. This finding corroborates the results of the synthetic experiment conducted by Sun et al. (2013), who suggested that a slightly higher than the normal S_s value can offset the influence of incorrectly assigned constant head boundary. Conversely, when the true constant head boundary is erroneously designated as a no flux boundary, the impacts on the estimated S_s values in the vicinity of the boundaries are inconsistent. An anomalously high S_s zone emerges at the right boundary (right bottom plates in Fig. 6b) while the S_s values remain unchanged (or slightly small) at the left boundary (left bottom plates in Fig. 6b). This is because both high and low anomalous S_s values can be used to mimic the constant head boundary condition. The high S_s anomaly behaves as a water tank and the low S_s anomaly acts as a preferential flow pathway.

In summary, the results of identifying the boundary conditions of an aquifer through the sandbox experiments indicate that the transient state HT is more effective than the steady state HT in identifying incorrectly assigned boundaries. This finding differs from that reported by Liu et al. (2020) who employed noise-free synthetic experiments. The discrepancies can be attributed to the inclusion or exclusion of noise in

the analysis. In theory, the steady state HT is more effective in identifying the unknown boundary than the transient state HT because the steady state inversion requires less amount of constraint than the transient state inversion to formulate a well-defined problem (Mao et al., 2013; Yeh et al., 2015). However, real-world experiments inherently include measurement noise, such as random fluctuations and systematic errors from sensors. The steady state measurements corrupted by noise can have a profound effect on inversion (Illman et al., 2007). Transient measurements can mitigate the effects of random noise and potentially reduce estimation uncertainties (Wang et al., 2017).

3.2. Effects of well location and density on identifying the type of boundary

The anomalous K values estimated using different well densities are effective in identifying the unknown no flux boundary. Fig. 7 illustrates the percentage differences of estimated K values between the incorrectly assigned and true boundary conditions using 45 (scenarios 4–6), 15 (scenarios 7–9), and 10 (scenarios 10–12) wells. A comparison of the percentage differences of K values using different densities of pumping and observation wells reveals that the influences of incorrectly assigned constant head boundaries on the flow field are offset by the presence of low permeable zones (blue colors adjacent to the middle plate).

Fig. 8 shows the percentage differences of estimated S_s values between the incorrectly assigned and true boundary conditions using 45 (scenarios 4–6), 15 (scenarios 7–9), and 10 (scenarios 10–12) wells. The percentage differences of S_s values show that in all well densities, high S_s zones emerge along the boundaries with incorrectly assigned constant head values (red colors adjacent to the middle plate). In addition, both anomalous high and low S_s values can be used to mimic the constant head boundary condition. When the constant head boundary is incorrectly assigned as the no flux boundary, the anomalous high and low S_s zones manifest in proximity to these boundaries (Fig. 8d, e, and f). These findings align with those depicted in Fig. 6b.

The density of wells has an influence on the effectiveness of HT when using the S_s anomalies to ascertain the boundary condition. As the well

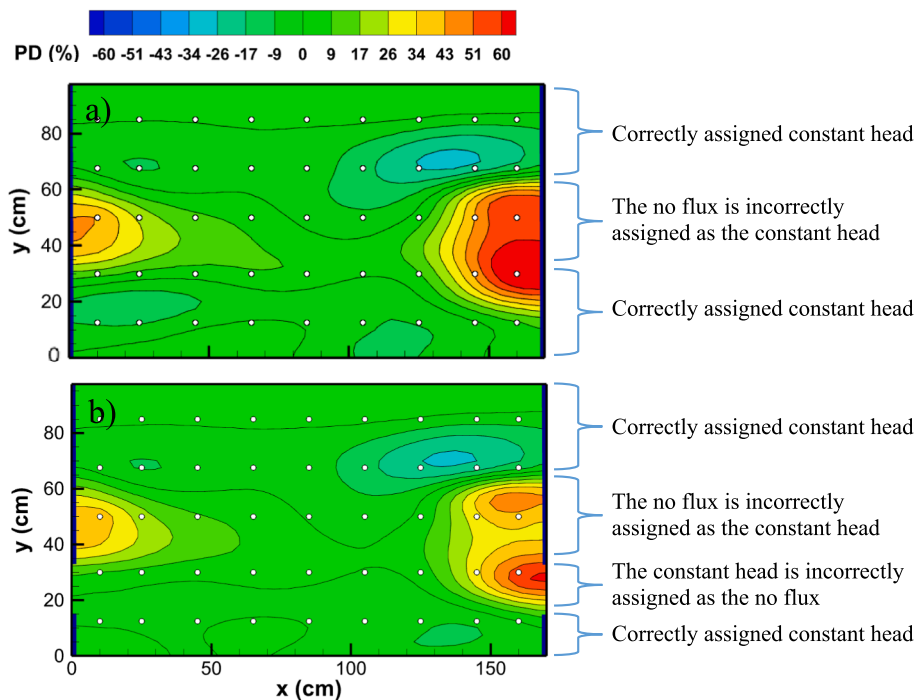


Fig. 6. The percentage differences of estimated S_s values between the true and incorrectly assigned boundary conditions using the transient state pumping tests. The white circles represent the wells. The bold solid lines indicate the constant head boundaries. The remaining boundaries are no flux.

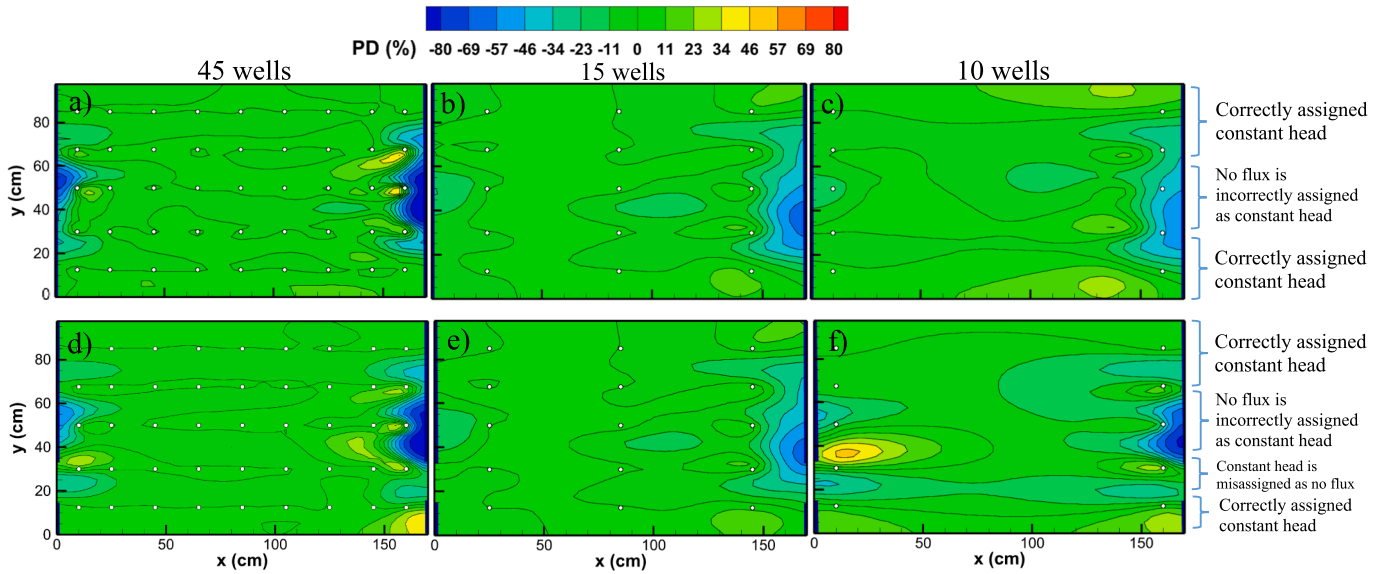


Fig. 7. The percentage differences of K tomograms using 45, 15, and 10 wells. The upper row (a, b, c) presents the percentage differences when the middle plates are incorrectly placed as the wrong boundaries. The lower row (d, e, f) shows the percentage differences when the wrong boundaries are assigned to the middle and the upper half of bottom plates. The white circles represent the wells. The bold solid lines indicate the constant head boundaries. The remaining boundaries are no flux.

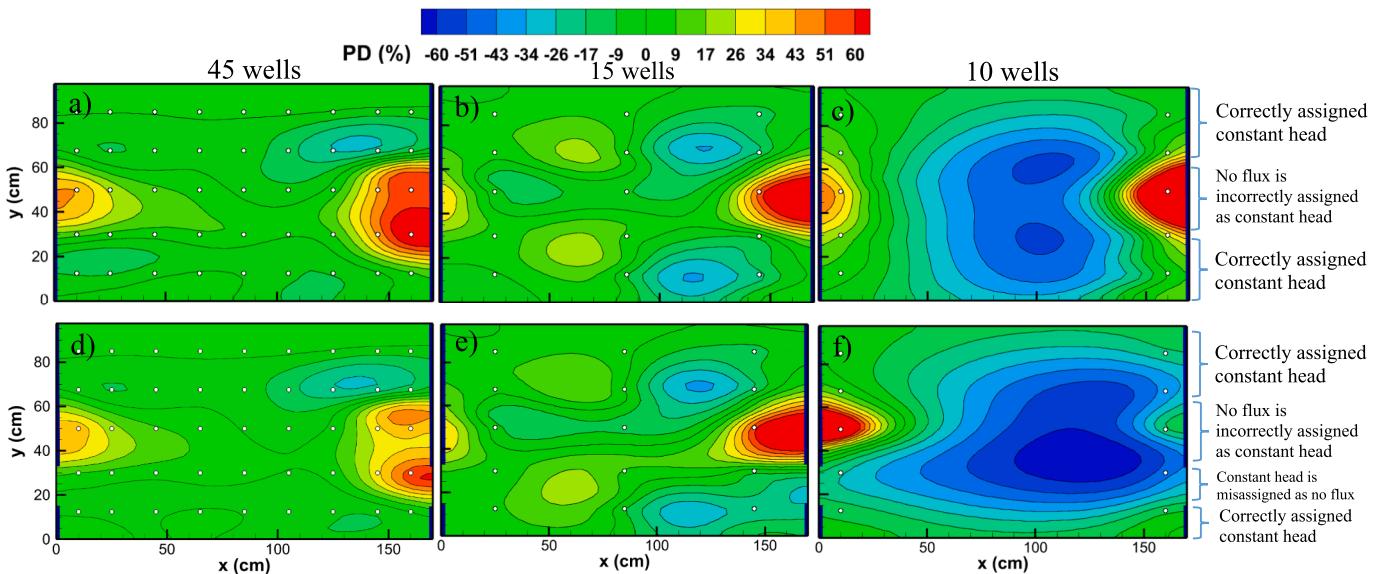


Fig. 8. The percentage differences of S_s tomograms using 45, 15, and 10 wells. The upper row presents the percentage differences when the middle plates are incorrectly placed as the wrong boundaries. The lower row shows the percentage differences when the wrong boundaries are assigned to the middle and the upper half of bottom plates. The white circles represent the wells. The bold solid lines indicate the constant head boundaries. The remaining boundaries are no flux.

density decreases, the S_s estimates located in the central region of the domain exhibit considerable fluctuations. This increases uncertainty in identifying the boundary location. A comparison of the percentage differences of estimated S_s values using all wells (Fig. 8a and d) and 15 wells (Fig. 8b and e) reveals that the percentage differences using 15 wells are greater (more reddish and bluish colors) at regions without observation wells. The use of drawdown data from only 10 wells gives an even more pronounced percentage difference (bluish colors in Fig. 8c and f). These relative high or low S_s anomalies may be misinterpreted as the no flux or constant head boundary. On the contrary, the well density does not affect the estimated K values. The percentage differences of estimated K values between the incorrectly assigned and true boundaries using different well densities remain similar (Fig. 7). Even in the

regions distant from the observation wells, the estimates remain consistent (greenish colors).

The reliability of K and S_s estimates using different well densities can be explained by the sensitivity of head with respect to K and S_s values. A high sensitivity value indicates that the observed head likely provides more inference to the unknown parameter than the observations with a low sensitivity value. The sensitivities are calculated by summing up the sensitivity values of all possible pairs of observation and pumping wells. Fig. 9 illustrates the spatial distribution of highly sensitive wells with respect to both K and S_s , K only, and S_s only. The top 20 wells with the highest sensitivity values are considered to be highly sensitive. Wells marked in green indicate high sensitivity for both K and S_s , while those marked in blue indicate high sensitivity for K only and those marked in

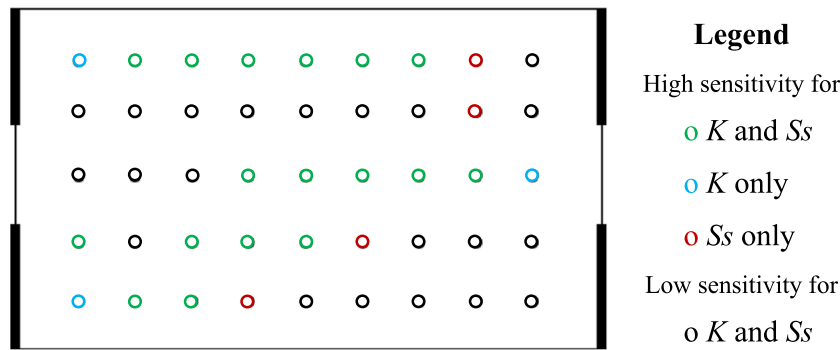


Fig. 9. The spatial distribution of different levels of sensitivity with respect to K and S_s . The circles represent the wells. The bold solid lines indicate the constant head boundaries. The remaining boundaries are no flux.

red indicate high sensitivity for S_s only. Wells not marked are considered to be low-sensitive wells for both K and S_s . The wells with high sensitivity (the blue and green wells in Fig. 9) and low sensitivity (the red and black wells) for K are evenly distributed throughout the aquifer. In contrast, the wells near the constant head boundaries are all considered to be low sensitivity for S_s (the blue and black wells). In geostatistical inversion, the aquifer hydraulic information embedded in the measurement is transferred to the parameters through sensitivity. A low sensitivity value amplifies the impact of uncertainty (e.g., uncertain boundary conditions, measurement noise, etc.) on the estimated parameters. As the wells with low sensitivity for S_s are located next to the boundaries, the measurements collected from these wells are ineffective to offset the effects of uncertain boundary conditions. As the number of wells decreases, the effects of uncertainty on the inversion become increasingly challenging. Consequently, it may be difficult to use the anomalous S_s values alone to identify the unknown boundary conditions (Figs. 7 and 8). It is essential to consider both anomalous K and S_s values simultaneously.

3.3. Identify the unknown aquifer geometry and boundary type in the extended domain

In practice, an extended domain that encompasses a larger area than the site is typically utilized to address the challenge of uncertain aquifer geometry and boundary conditions. Therefore, we further explore to what extent do the anomalous K and S_s delineate the aquifer boundary within the extended domain.

The estimated K and S_s fields over the extended aquifer are presented in Fig. 10 (scenario 13). The effects of unknown aquifer geometry on estimated K and S_s values along the true boundary locations are summarized in Table 2. A close examination around the K and S_s tomograms indicates that the relatively low K and S_s zones appear near the top and bottom boundaries of the extended domain. The low K zones act as

impermeable barriers to prevent the water from moving into the aquifer. The low S_s anomalies indicate a reduction in the quantity of water stored in these regions. These low K and S_s anomalies are indicative of the locations of no flux boundaries. These findings are in line with the synthetic experiments conducted by Liu et al. (2020) and Daranond et al. (2020).

On the other hand, it is challenging to portray the unknown location and type of constant head boundary condition using the anomalous K and S_s values. The anomalous high K and S_s values do not manifest near the locations of true constant head boundaries. These findings diverge from the synthetic experiment by Liu et al. (2020) who concluded that the extremely high K and S_s anomalies emerge in the extended domain to emulate the constant head boundary. The reason for this discrepancy is unclear and warrants further investigation.

4. Conclusions

This study investigates the potential of hydraulic tomography in identifying unknown aquifer geometry and boundary conditions using a sandbox experiment. The scenarios analyzed include combinations of incorrectly assigned constant head and no flux boundaries, steady and transient state measurements, different well densities and locations, and an extended domain broader than the size of the sandbox. We conclude that:

(1) The anomalies K and S_s values serve as indicators of the no flux boundary. When the no flux boundary is incorrectly assigned as the constant head, the low K and high S_s anomalous zones emerge in the vicinity of the boundary. The low K zones act as impermeable barriers and the high S_s anomaly behaves as a water tank to prevent the water from flowing into the sandbox.

(2) It is ineffective to use K and S_s to identify the constant head boundary when it is incorrectly assigned as the no flux. The estimated K values remain similar to those using the correct one, while both

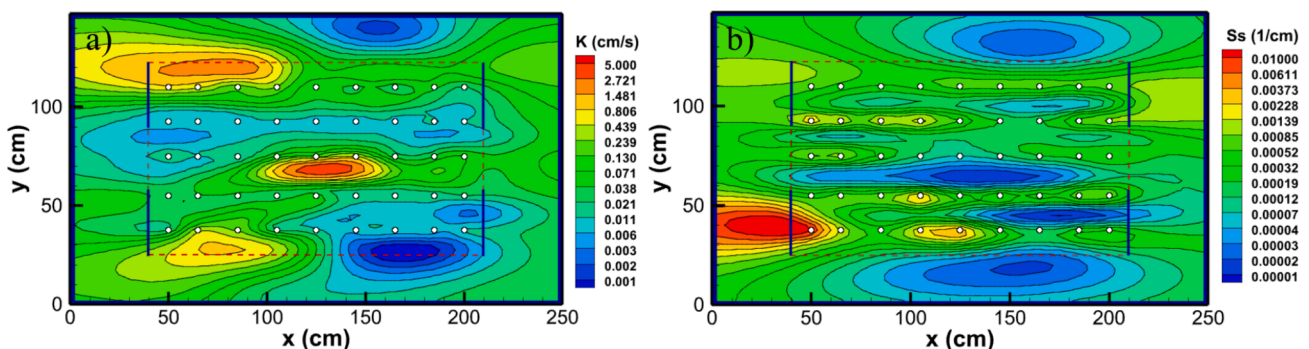


Fig. 10. The K and S_s tomograms using the extended domain. The white circles represent the wells. The bold solid lines indicate the constant head boundaries. The remaining boundaries are no flux. The red dashed lines and the blue solid lines next to the wells represent the locations of correct boundary.

anomalous high and low S_s manifest to emulate the constant head boundary. Therefore, when the boundary condition is unknown, a constant head boundary should be used to prevent misinterpretation.

(3) The transient state HT provides a more reliable assessment of boundary conditions than the steady state HT. The partially redundant temporal measurements offset the influences of measurement noise on the estimate.

(4) The well density partially affects the ability of HT to identify the boundary condition. As the well density decreases, the K estimates remain similar while the S_s estimates located in the central region of the domain exhibit considerable fluctuations. The wells with high and low sensitivities for K are evenly distributed throughout the aquifer. In contrast, the wells near the constant head boundaries are all considered to be low sensitivity for S_s . Therefore, the measurements collected from these wells are ineffective to offset the effects of uncertain boundary conditions. As the number of wells decreases, the effects of uncertainty on the inversion become increasingly challenging.

(5) The HT is effective in identifying no flux boundary conditions when both aquifer geometry and type of boundary are unknown. The low K and S_s anomalies manifest near the locations where no flux boundary should be. On the contrary, identifying the constant head boundaries remains challenging. The K and S_s anomalies did not clearly correspond to the actual locations of the constant head boundary. Therefore, in real-world applications involving complex aquifers with unknown geometry and boundary conditions, using a constant head boundary helps prevent misinterpretation.

Declaration of Generative AI and AI-assisted technologies in the writing process

During the preparation of this work the authors used GPT and DeepL in order to improve the readability and language of the manuscript. After using this tool/service, the authors reviewed and edited the content as needed and takes full responsibility for the content of the published article.

CRediT authorship contribution statement

Mpendulo Mangaliso Mtsetfwa: Writing – original draft, Visualization, Methodology, Formal analysis. **Zaiyong Zhang:** Writing – review & editing, Funding acquisition. **Chengcheng Gong:** Writing – review & editing, Visualization, Funding acquisition. **Hong-Ru Lin:** Visualization, Investigation, Data curation. **Jet-Chau Wen:** Writing – review & editing, Funding acquisition. **Yu-Li Wang:** Writing – review & editing, Writing – original draft, Visualization, Validation, Supervision, Software, Methodology, Funding acquisition, Formal analysis, Conceptualization.

Declaration of competing interest

The authors declare that they have no known competing financial interests or personal relationships that could have appeared to influence the work reported in this paper.

Acknowledgments

We gratefully acknowledge the support of the following grants: National Key R&D Program of China (2020YFC1808302-004), Fund Program for the Scientific Activities of Selected Returned Overseas Professionals in Shaanxi Province (2020006), Fundamental Research Funds for the Central Universities CHD (2024SHEEAR002 and 300102292201), China Postdoctoral Science Foundation (GZC20232955, 2024M753472, and 2024MD763937), Science-Tech- nology Foundation for Young Scientists of Gansu Province (24JRRA097), and Taiwan National Science and Technology Council grant NSTC113-2221-E-002-081. We would also like to acknowledge the

funding provided by the Agricultural Net-Zero Carbon Technology and Management Innovation Research Center at National Taiwan University. The authors thank the editors and reviewers for their helpful and insightful comments, which have significantly improved the quality of this paper.

Data availability

Data will be made available on request.

References

- Adeyeri, O.E., Zhou, W., Ndehedehe, C.E., Wang, X., Ishola, K.A., Laux, P., 2024. Minimizing uncertainties in climate projections and water budget reveals the vulnerability of freshwater to climate change. *One Earth* 7 (1), 72–87. <https://doi.org/10.1016/j.oneear.2023.12.013>.
- Bastani, M., Harter, T., 2020. Effects of upscaling temporal resolution of groundwater flow and transport boundary conditions on the performance of nitrate-transport models at the regional management scale. *Hydrogeol. J.* 28, 1299–1322. <https://doi.org/10.1007/s10040-020-02133-x>.
- Coelho, C.D., Faria, A.C.S., Marques, E.A.G., 2017. Comparative analysis of different boundary conditions and their influence on numerical hydrogeological modeling of Palmital watershed, southeast Brazil. *J. Hydrol. Reg. Stud.* 12, 210–219. <https://doi.org/10.1016/j.ejrh.2017.05.006>.
- Dagan, G., 1985. Stochastic modeling of groundwater flow by unconditional and conditional probabilities: the inverse problem. *Water Resour. Res.* 21 (1), 65–72. <https://doi.org/10.1029/WR021i001p0065>.
- Daranond, K., Yeh, T.-C.-J., Hao, Y., Wen, J.-C., Wang, W., 2020. Identification of groundwater basin shape and boundary using hydraulic tomography. *J. Hydrol.* 588, 125099. <https://doi.org/10.1016/j.jhydrol.2020.125099>.
- Gao, X., Yan, E.C., Yeh, T.-C.-J., Wang, Y.-L., Liang, Y., Hao, Y., 2018. Reliability analysis of hydrologic containment of underground storage of liquefied petroleum gas. *Tunn. Undergr. Space Technol.* 79, 12–26. <https://doi.org/10.1016/j.tust.2018.04.037>.
- Gao, X., Yeh, T.-C.-J., Yan, E.C., Wang, Y.-L., Hao, Y., 2021. Conditional mean, effective, and realizations of hydraulic conductivity fields. *J. Hydrol.* 592, 125606. <https://doi.org/10.1016/j.jhydrol.2020.125606>.
- Hartmann, A., Gleeson, T., Wada, Y., Wagener, T., 2017. Enhanced groundwater recharge rates and altered recharge sensitivity to climate variability through subsurface heterogeneity. *Proc. Natl. Acad. Sci. (PNAS)* 114 (11), 2842–2847. <https://doi.org/10.1073/pnas.1614941114>.
- Ho, Y.-T., Wang, Y.-L., Chang, L.-C., Wang, T.-P., Tsai, J.-P., 2021. Optical system for monitoring groundwater pressure and temperature using fiber Bragg gratings. *Opt. Express* 29, 16032–16045. <https://doi.org/10.1364/OE.412518>.
- Illman, W., Liu, X., Craig, A., 2007. Steady-state hydraulic tomography in a laboratory aquifer with deterministic heterogeneity: Multi-method and multiscale validation of hydraulic conductivity tomograms. *J. Hydrol.* 341, 222–234. <https://doi.org/10.1016/j.jhydrol.2007.05.011>.
- Irsa, J., Zhang, Y., 2012. A direct method of parameter estimation for steady state flow in heterogeneous aquifers with unknown boundary conditions. *Water Resour. Res.* 48 (9). <https://doi.org/10.1029/2011WR011756>.
- Jiao, J., Zhang, Y., 2014a. Two-dimensional physical-based inversion of confined and unconfined aquifers under unknown boundary conditions. *Adv. Water Resour.* 65, 43–57. <https://doi.org/10.1016/j.advwatres.2013.10.011>.
- Jiao, J., Zhang, Y., 2014b. A method based on local approximate solution (LAS) for inverting transient flow in heterogeneous aquifers. *J. Hydrol.* 514, 145–149. <https://doi.org/10.1016/j.jhydrol.2014.04.004>.
- Jiao, J., Zhang, Y., 2015. Tensor hydraulic conductivity estimation for heterogeneous aquifers under unknown boundary conditions. *Groundwater* 53 (2), 293–304. <https://doi.org/10.1111/gwat.12202>.
- Kitanidis, P.K., Vomvoris, E.G., 1983. A geostatistical approach to the inverse problem in groundwater modeling (steady state) and one-dimensional simulations. *Water Resour. Res.* 19 (3), 677–690. <https://doi.org/10.1029/WR019i003p0677>.
- Kitanidis, P.K., 1995. Quasi-linear geostatistical theory for inverting. *Water Resour. Res.* 31 (10), 2411–2419. <https://doi.org/10.1029/95WR01945>.
- Lin, H.-R., Wen, J.-C., Zhang, Z., Wang, Y.-L., 2023. Characterizing basin-scale subsurface hydraulic heterogeneity with multiscale geological and hydrological measurements. *J. Hydrol.* 625, 130061. <https://doi.org/10.1016/j.jhydrol.2023.130061>.
- Liu, F., Yeh, T.-C.-J., Wang, Y.-L., Song, X., Lei, X., Wen, J.-C., Wang, W., Hao, Y., 2020. Potential of hydraulic tomography in identifying boundary conditions of groundwater basins. *Water Resour. Res.* 56, e2020WR028331. <https://doi.org/10.1029/2020WR028331>.
- Mao, D., Yeh, T.-C.-J., Wan, L., Hsu, K.-C., Lee, C.-H., Wen, J.-C., 2013. Necessary conditions for inverse modeling of flow through variably saturated porous media. *Adv. Water Resour.* 52, 50–61. <https://doi.org/10.1016/j.advwatres.2012.08.001>.
- Michael, H.A., Khan, M.R., 2016. Impacts of physical and chemical aquifer heterogeneity on basin-scale solute transport: vulnerability of deep groundwater to arsenic contamination in Bangladesh. *Adv. Water Resour.* 98, 147–158. <https://doi.org/10.1016/j.advwatres.2016.10.010>.
- Priestley, M. B. (1982). *Spectral Analysis and Time Series, Two-Volume Set (1st ed., Vols. I and II)*. ISBN: 9780125649223.

- Ren, S., Zhang, Y., Jim Yeh, T.-C., Wang, Y., Carr, B.J., 2021. Multiscale hydraulic conductivity characterization in a fractured granitic aquifer: the evaluation of scale effect. *Water Resour. Res.* 57, e2020WR028482. <https://doi.org/10.1029/2020WR028482>.
- Su, X., Yeh, T.-C.-J., Li, K., Wang, G., Wang, Z., 2024. Optimal strategies for assigning prior boundary settings in Hydraulic Tomography analysis. *Adv. Water Resour.* 186, 104674. <https://doi.org/10.1016/j.advwatres.2024.104674>.
- Sun, N.-Z., Yeh, W.-W.-G., 1990. Coupled inverse problems in groundwater modeling: 1. Sensitivity analysis and parameter identification. *Water Resour. Res.* 26 (10), 2507–2525. <https://doi.org/10.1029/WR026i10p02507>.
- Sun, R., Yeh, T.-C.-J., Mao, D., Jin, M., Lu, W., Hao, Y., 2013. A temporal sampling strategy for hydraulic tomography analysis. *Water Resour. Res.* 49, 3881–3896. <https://doi.org/10.1002/wrcr.20337>.
- Sykes, J.F., Wilson, J.L., Andrews, R.W., 1985. Sensitivity analysis for steady-state groundwater flow using adjoint operators. *Water Resour. Res.* 21 (3), 359–371. <https://doi.org/10.1029/WR021i003p00359>.
- Wang, Y.-L., Yeh, T.-C.-J., Wen, J.-C., Huang, S.-Y., Zha, Y., Tsai, J.-P., Hao, Y., Liang, Y., 2017. Characterizing subsurface hydraulic heterogeneity of alluvial fan using riverstage fluctuations. *J. Hydrol.* 547, 650–663. <https://doi.org/10.1016/j.jhydrol.2017.02.032>.
- Wang, Y.-L., Yeh, T.-C.-J., Wen, J.-C., Gao, X., Zhang, Z., Huang, S.-Y., 2019. Resolution and ergodicity issues of river stage tomography with different excitations. *Water Resour. Res.* 55, 4974–4993. <https://doi.org/10.1029/2018WR023204>.
- Wang, Y.-L., Yeh, T.-C.-J., Xu, D., Li, K., Wen, J.-C., Huang, S.-Y., Wang, W., Hao, Y., 2021. Stochastic analysis of oscillatory hydraulic tomography. *J. Hydrol.* 596, 126105. <https://doi.org/10.1016/j.jhydrol.2021.126105>.
- Wang, Y.-L., Yeh, T.-C.-J., Liu, F., Wen, J.-C., Wang, W., Hao, Y., 2022. Characterize basin-scale subsurface using rocket-triggered lightning. *Geophys. Res. Lett.* 49, e2022GL101278. <https://doi.org/10.1029/2022GL101278>.
- Yeh, T.-C.-J., Khaleel, R., Carroll, K.C., 2015. *Flow Through Heterogeneous Geologic Media*. Cambridge University Press. <https://doi.org/10.1017/CBO9781139879323>.
- Yeh, T.-C., Gutjahr, A.L., Jin, M., 1995. An iterative cokriging-like technique for groundwater flow modeling. *Groundwater* 33 (1), 33–41. <https://doi.org/10.1111/gwat.1995.33.issue-1>.
- Zhang, Y., 2014. Nonlinear inversion of an unconfined aquifer: Simultaneous estimation of heterogeneous hydraulic conductivities, recharge rates, and boundary conditions. *Transp. Porous Media* 102 (2), 275–299. <https://doi.org/10.1007/s11242-014-0275-x>.
- Zhang, Y., Irsa, J., Jiao, J., 2014. Three-dimensional aquifer inversion under unknown boundary conditions. *J. Hydrol.* 509, 416–429. <https://doi.org/10.1016/j.jhydrol.2013.11.024>.
- Zhang, Z., Wang, W., Gong, C., Yeh, T.-C.-J., Wang, Z., Wang, Y.-L., Chen, L., 2018. Finite analytic method for modeling variably saturated flows. *Sci. Total Environ.* 621, 1151–1162. <https://doi.org/10.1016/j.scitotenv.2017.10.112>.
- Zhang, Z., Yang, J., Gong, C., Wang, W., Ran, B., Wang, G., Zhang, Q., Wang, Y.-L., 2024. Enhancing predictions of remedial reagent transport via a vertical groundwater circulation well with high-resolution aquifer characterization. *Sci. Total Environ.*, 171041 <https://doi.org/10.1016/j.scitotenv.2024.171041>.